



# Technical note: Measurements and data analysis of sediment-water oxygen flux using a new dual-optode eddy covariance instrument.

Markus Huettel<sup>1</sup>, Peter Berg<sup>2</sup>, Alireza Merikhi<sup>1</sup>

<sup>1</sup> Department of Earth, Ocean and Atmospheric Science, Florida State University, Tallahassee, FL 32306-4520, USA

<sup>2</sup> Department of Environmental Sciences, University of Virginia, Charlottesville, VA 22904-4123, USA

*Correspondence to:* Markus Huettel (mhuettel@fsu.edu)

**Abstract.** Sediment-water oxygen fluxes are widely used as a proxy for organic carbon production and mineralization at the seafloor. In-situ fluxes can be measured non-invasively with the aquatic eddy covariance technique, but a main weakness of the commonly used instrumentation is the susceptibility of the delicate oxygen microsensors required for the high frequency measurements to disturbances. Even small changes in sensor characteristics during deployment as caused e.g. by biofouling can result in erroneous flux data. Here we present a dual-optode eddy covariance instrument (2OEC) with two fast oxygen fiber sensors and document how erroneous flux interpretations and data loss can effectively be reduced by this hardware and a new data analysis approach. With deployments over a carbonate sandy sediment in the Florida Keys and comparison with parallel benthic advection-chamber incubations, we demonstrate the improved data quality and data reliability facilitated by the instrument and associated data processing. Short-term changes in flux that are questionable in single oxygen sensor instruments can be confirmed or rejected with the 2OEC and in our deployments provided new insights into the temporal dynamics of benthic oxygen flux in permeable carbonate sands. With the 2OEC, reliable benthic flux data can be generated within a couple of hours, making this technique suitable for mapping sediment-water, intra-water column, or atmosphere-water fluxes.

## 20 1 Introduction

The significant role of sediments in the marine cycles of matter (Walsh, 1988; Johnson et al., 1999; Jahnke, 2010; Bauer et al., 2013) emphasizes the need for reliable benthic flux data. Where currents and benthic photosynthesis influence oxygen flux at the seafloor, the aquatic eddy covariance technique (Fig. 1) is a preferred tool for determining benthic oxygen fluxes as it permits flux measurements with minimal disturbance of bottom flow and light. This technique derives vertical oxygen flux from time series of rapid simultaneous measurements of vertical flow velocity changes and associated oxygen changes at a fixed point above the sediment surface. Since its introduction by Berg et al. (2003), the strength of this non-invasive technique has been demonstrated in marine and freshwater settings (Berg et al., 2013; Chipman et al., 2016; Hume et al., 2011; Reimers et al., 2012a; Rheuban et al., 2014a; Lorrai et al., 2010; Attard et al., 2019; Rodil et al., 2019) including environments (e.g. permeable sediments, seagrass beds, coral reefs, hard bottoms, sea ice) that pose challenges to other flux-measuring techniques (Berg et al., 2009; Brand et al., 2008; Crusius et al., 2008; Glud et al., 2010; McGinnis et al., 2014; Berg and Pace, 2017; Long et al., 2013; Long et al., 2012; Berger et al., 2020).



The main challenge of the present aquatic eddy covariance instrumentation is associated with the high frequency oxygen measurements. The microelectrodes typically used for these measurements (sensor tip < 100  $\mu\text{m}$ ), break easily during 35 deployments in energetic coastal environments (Chipman et al., 2012; Berg et al., 2017), and their stirring sensitivity and signal drift add further uncertainties to the oxygen data (Gundersen et al., 1998; Holtappels et al., 2015).

An alternative to the electrochemical microelectrodes are optical sensors (optodes or optrodes) that use the luminescence characteristics of an oxygen-sensitive dye for oxygen concentration measurements (Klimant et al., 1995; Holst et al., 1998; 40 Bittig et al., 2018; Wang and Wolfbeis, 2014). Optodes consume no oxygen and have very low or no stirring sensitivity (Holtappels et al., 2015). Compared to microelectrodes, they are less susceptible to signal drift and keep their calibration over longer time. Because they are not sensitive to sulfides, optodes are the superior sensor in hypoxic environments or near anoxic sediment surfaces. Weaknesses of optodes include the bleaching of the sensor dye over time, their non-linear calibration with 45 decreasing resolution at high oxygen concentrations, and interference of strong light with the optical measurements (Lehner et al., 2015). In long-term measurements, the bleaching effect can be reduced through interval measurements. The non-linear calibration can be described by a function based on the Stern-Volmer equation (Stern and Volmer, 1919; Wang and Wolfbeis, 2014) that allows reliable conversion of the optode signal to concentration data, but the decreasing resolution at high oxygen concentrations remains. The light interferences typically are only an issue in very shallow water and can be eliminated by protective fiber coatings.

50

Irrespective of the technology, the oxygen sensors are affected by biofouling. Marine snow particles, bacteria and algae attaching to the sensing tip can affect the sensor signal through shielding of the sensor tip from the water current and metabolic processes (i.e. respiration, photosynthesis) (Smith et al., 2007; Delauney et al., 2010). While substantial biofouling may be 55 obvious through the changes in signal magnitude and dynamics it causes, minor biofouling is not detectable without a reference. Small deviations in the response time and magnitude of the sensor signal, however, can produce large differences between the measured and true flux (Berg et al., 2015). Some biofouling can be reduced by coating the sensor with antibiotics but such treatments cannot prevent the adherence of marine snow or detritus particles (Navarro-Viloslada et al., 2001).

With the advantages of being mechanically more robust and less expensive than microelectrodes, optodes are predisposed to 60 become the preferable sensor-type for aquatic eddy covariance measurements (Chipman et al., 2012; Berg et al., 2016). The recent development of small, programmable oxygen meters with low power consumption that can read fiber optodes with short response times made optode technology suitable and accessible for aquatic eddy covariance measurements. The goals of this study were 1) to develop an eddy covariance instrument with dual optodes that through parallel oxygen measurements allows 65 improved quality control of the oxygen data and thereby more reliable oxygen fluxes, 2) to develop a data evaluation procedure for the dual optode eddy covariance data sets that helps identifying compromised optode signals, 3) to demonstrate the



performance of this instrument through deployment in an inner shelf environment with dynamic changes in sediment-water flux.

## 2 Methods

### 2.1 Instrument development

70 The eddy covariance instrument we developed uses two Pyroscience™ FireSting O<sub>2</sub>-Mini oxygen meters (specifications listed in Table A1 in Appendix A) that read two ultra-high speed Pyroscience™ OXR430-UHS retractable oxygen minisensors (Table A2). The measuring principle of the Pyroscience™ fiber optodes is based on an indicator dye responding to orange-red light excitation (610-630 nm) and lifetime detection in the near infrared (NIR, 760-790 nm), which reduces cross-sensitivity and interferences (e.g. due to ambient light or fluorescent substances in the water). The ultra-high speed OXR430-UHS optodes  
75 achieve response times ( $t_{90}$ ) of 150 to 300 ms (Merikhi et al., 2018) and thus can easily capture oxygen fluctuations at the temporal resolution required by the eddy covariance technique (Lorrai et al., 2010; Donis et al., 2015), preventing loss of flux contributions at high turbulence frequencies (McGinnis et al., 2008b). The 430  $\mu\text{m}$  diameter optical fiber of these optodes is relative robust relative to microelectrodes. When operated continuously at a measuring frequency of  $\sim 8$  Hz, the useful lifetime of the OXR430-UHS typically was 3 to 7 days before the signal decreased to a level precluding reliable data interpretation.  
80 The signal drift over this period was negligible (< 0.03%). The optodes for the in-situ measurements were selected for similar fast response times (< 300 ms) using the jet-nozzle method introduced by Merikhi et al. (2018). The acoustic Doppler velocimeter (ADV) used for this eddy instrument was a NORTEK Vector, which is a single-point current meter capable of measuring velocity and current direction in a small measuring volume (14 mm diameter, 14 mm height (user-specified)), at rates up to 64 Hz (Table A3). Together with the current flow measurements, the Vector records pressure and temperature, as  
85 well as the compass direction and tilt of the instrument. The internal data logger of the Vector stored the current velocity data simultaneously with the two analogue signals produced by the O<sub>2</sub>Mini oxygen meters. An external battery with a capacity of 200 Wh connected to the Vector provided power for continuous measurements of up to one week duration.

90 The instruments were mounted on a tripod (width 120 cm, height 100 cm, Fig. 1), made of rectangular 304-stainless steel tubes (2 cm x 2 cm cross-section), with legs consisting of stainless steel rods, 1.3 cm in diameter with 20 cm diameter base plates. An extension arm held the ADV in the center of the frame. The underwater housing (AGO Environmental Electronics) containing the oxygen meters with supply voltage regulator (Dimension Engineering) and the external battery pack (4 x NORTEK Lithium-Ion 12 V, 50 Wh) were attached to the horizontal upper bar of the tripod. All electrical cables used Impulse™ wet pluggable micro inline connectors. The two optodes were linked through two custom-made (Huettel) underwater housing fiber-feed-through plugs with standard ST-connectors to the FireSting O<sub>2</sub>Minis. A stainless steel rod (8 mm diam.) with adjustable holders and aligned with the X-direction of the ADV, positioned the two optodes at a 45-degree downward angle such that their measuring tips were located at 30 mm horizontal distance from the lower edge of the ADV  
95



measuring volume and 10 mm horizontally apart from each other. A PAR-light sensor (Odyssey® Submersible Photosynthetic Active Radiation Logger) installed above the ADV logged light intensity at 5 minute intervals throughout the 100 deployments. An Aanderaa Seaguard RCM multisensory probe, installed with its sensors at the same height as the ADV measuring volume at 5 m distance from the tripod, recorded oxygen and temperature reference data.

## 2.2 Field tests

The performance of the 2OEC was tested through three deployments (August 14-15 and 16-17 2013, and April 10-11, 2014) in a subtropical inner shelf environment with relatively constant salinity (35-36) and temperatures (April:  $25^\circ \pm 0.8^\circ\text{C}$ , August: 105  $30^\circ \pm 0.5^\circ\text{C}$ ) approximately 9 km south of Long Key in the Florida Keys ( $24^\circ 43.52'\text{N}$ ,  $80^\circ 49.85'\text{W}$ ). The site was located at  $9 \pm 1$  m water depth near the center of a large flat carbonate platform covered with coral sand. The unobstructed, fairly steady current flows across the platform and the relatively uniform surface roughness (ripple topography  $< 10$  cm) produced similar turbulent diffusivity throughout the deployments. The highly permeable carbonate sand (permeability:  $k = 3 \times 10^{-11} \pm 0.2 \times 10^{-11}$  110  $\text{m}^2$ ) had a median grain size of 440  $\mu\text{m}$  and was inhabited by microphytobenthos ( $2\text{-}6 \mu\text{g Chl. a g}^{-1} \text{ sed. dw}$ ) and sparsely distributed ( $< 20 \text{ m}^{-2}$ ) *Halimeda* sp. Macroalgae (Fig. 1A). In the clear water (Turbidity  $< 8$  NTU) light intensities at the seafloor reached up to  $300 \mu\text{E m}^{-2} \text{ s}^{-1}$ . The current flow conditions during all deployments were moderate (average mean flow velocity 5 to 20  $\text{cm s}^{-1}$ , significant wave height  $< 0.7$  m), and the weather was generally sunny with some scattered clouds. Prior to the deployments, the oxygen optodes were calibrated in ambient seawater (water bubbled with air or with sodium 115 sulfite addition), with the calibration data stored on the Vector logger. The measuring volume of the ADV was adjusted to be  $\sim 35$  cm above the sediment-water interface. SCUBA divers positioned the instrument at the seafloor such that the Vector's X-direction was aligned with the main bottom flow direction, which was in northeast-southwest direction. The instrument was typically deployed in the morning at 9:00-10:00 and retrieved 24 h later. During the first hour after deployment, no flux data were collected to allow temperature adjustment of the instruments. Before downloading the data from the Vector, the calibration of the oxygen sensors was repeated and stored with the data file.

## 120 2.3 Data processing

Velocity data with acoustic beam correlations  $< 50\%$  were replaced through linear interpolation of the neighboring velocity values. Oxygen data were not cleaned or despiked prior to flux calculations. Oxygen fluxes were calculated using EddyFlux 3.2 software package (P. Berg) as follows: Vertical velocity data and oxygen concentration data were reduced from 64 Hz to 8 Hz through averaging, which lessened data noise while maintaining sufficient resolution for resolving high-frequency eddies. 125 The fluctuating component of the oxygen concentrations was determined through Reynolds decomposition, i.e. oxygen base concentrations were determined for 15 min intervals through linear detrending and subtracted from the instantaneous oxygen data to arrive at the instantaneous oxygen fluctuations  $O_2'$ . Instantaneous vertical velocity change  $V_z'$  were determined through Reynolds decomposition analogous to the oxygen fluctuations. As a tilted position of the eddy instrument relative to the main flow direction can bias the magnitude of the vertical flux, we tested whether fluxes were influenced by tilt by rotating the



130 average flow velocity vectors for 15 min intervals until the average  $V_z$  equalled zero. These tests indicated that tilt corrections  
were not required for our three deployments. Similarly, we tested whether wave rotation influenced flux by rotating flow  
velocity vectors until  $SD(v_y)$  and  $SD(v_z)$  ( $SD=1$  Standard Deviation) reached a minimum. Correction for wave rotation had a  
small effect and was applied in all data sets. The time lag caused by the 30 mm horizontal distance between flow and oxygen  
measurement locations and displacement of the vertical oxygen gradient by wave orbital motion were corrected according to  
135 Berg et al. (2015) through applying time shift corrections that yielded most negative (night) or most positive (day) cross-  
correlations of the oxygen fluctuation and vertical movement. Oxygen fluxes then were calculated by averaging over time the  
products instantaneous oxygen fluctuation and instantaneous vertical velocity change:  $O_2 Flux = \overline{O_2' \times V_z'}$  (Berg et al.,  
2003). Because large-scale variations in the average water column oxygen concentration (e.g. as caused by the diurnal changing  
balance of production and consumption processes) may not be captured by the turbulent eddy flux measurements (Rheuban et  
140 al., 2014b), an oxygen storage term, calculated as  $\int_0^h dC/dt h$ , was added to the eddy flux ( $dC/dt$  = change of the average oxygen  
concentration over time, calculated through linear detrending of the measured oxygen data over 15 minute intervals,  $h$  = height  
of the measuring volume). Acceleration or deceleration of current flows can alter the oxygen concentration profile and thereby  
modulate vertical flux (Holtappels et al., 2013). These temporal flux variations caused by transient velocity changes may  
largely cancel out over time (Rheuban et al., 2014b), as indicated in our study by the good agreement between the fluxes  
145 derived from the eddy covariance measurements and those recorded in parallel benthic advection chamber measurements. A  
correction for transient velocity changes was not applied. Error estimates are reported as  $\pm 1$  standard deviation.

## 2.4 Advection chamber deployments

In August 2013, 3 advection chambers were deployed parallel to the eddy covariance instrument to allow comparison with an  
independent flux data set produced by a different method. Benthic advection chambers present an in-situ incubation technique  
150 that can account for some of the current and light effects influencing benthic flux (Janssen et al., 2005a; Huettel and Gust,  
1992). The rotation of a stirring disk (15 cm diam.) within these cylindrical chambers (20 cm height, 19 cm diam.) is set  
according to flow and ripple dimensions to produce a radial pressure gradient ( $0-1 \text{ Pa cm}^{-1}$ ) at the surface of the enclosed  
sediment that is similar in magnitude to that produced by bottom currents interacting with present ripple topography (Huettel  
155 and Rusch, 2000). In highly permeable sediments, the pressure gradient in the chamber causes pore water flow through the  
surface layer of the enclosed sediment, thereby mimicking the pore water exchange occurring in the surrounding rippled  
seabed. The transparent chamber and stirring disk allow penetration of light to the enclosed sediment, facilitating benthic  
photosynthesis in the chamber. Although flow, light and water composition changes within the chamber are not identical to  
the external conditions and cause an inherent bias, the daily fluxes measured by these chambers are considered to be close  
160 (within a factor ~2) to the true fluxes (DeBeer et al., 2005; Cook et al., 2007; Janssen et al., 2005a), and this technique has  
been deployed successfully in numerous investigations of shallow permeable sediments (Huettel and Gust, 1992; Eyre et al.,  
2013; Eyre et al., 2018; Glud, 2008; Cyronak et al., 2013; Santos et al., 2011; Janssen et al., 2005b).



### 3 Results

#### 3.1 Instrument deployments

The 2OEC improves the reliability of measured fluxes. The deployment of 16-17 August 2013 was characterized by moderate bottom currents averaging  $3.6 \pm 2.2 \text{ cm s}^{-1}$  (35 cm above sediment) with sustained peak velocities of  $8.0 \text{ cm s}^{-1}$  (Fig. 2A) and relatively low light intensities at the seafloor  $< 100 \mu\text{E m}^{-2} \text{ s}^{-1}$  during daytime hours (Fig. 2E). The good agreement of the independent O<sub>2</sub> readings of both fiber optodes and the Seaguard reference optode (Fig. 2B) implied that the optodes maintained their calibration throughout the deployment. Identical corrections were applied to P and Q optode data sets when calculating fluxes (Fig. 2C), which included corrections for change in average water oxygen concentration, time lag, and wave rotation.

165 The conformity of the 15 min cumulative fluxes calculated from the two fiber optode signals (Fig. 2D) and the agreement of the cumulative flux curves over the time course of the deployment (Fig. 2E) corroborated the flux estimates. The slopes of the cumulative flux curves over the time course of the deployment (Fig. 2E) revealed day time fluxes of  $3.4 \pm 0.6 \text{ mmol m}^{-2} \text{ h}^{-1}$  (P) and  $3.4 \pm 0.4 \text{ mmol m}^{-2} \text{ h}^{-1}$  (Q) and night time fluxes of  $-1.3 \pm 0.9 \text{ mmol m}^{-2} \text{ h}^{-1}$  (P) and  $-1.6 \pm 0.9 \text{ mmol m}^{-2} \text{ h}^{-1}$  (Q). These close agreements between the fluxes calculated from the two optode signals supported an average day time flux of  $3.4 \pm 0.7 \text{ mmol m}^{-2} \text{ h}^{-1}$  (P, Q) and nighttime flux of  $-1.4 \pm 1.3 \text{ mmol m}^{-2} \text{ h}^{-1}$  (P, Q) for the 16-17 August deployment.

170

175

Analysis of the differences between optode P and optode Q based fluxes indicated that changes in environmental settings as well as changes in optode characteristics produced the discrepancies. Larger differences between the P and Q 15 minute fluxes were observed during daytime and when fluxes were near zero and changing direction at sunset (Fig. 3A). Patchy distribution 180 of microphytobenthos and its photosynthetic oxygen production may result in a more uneven oxygen distribution in the bottom currents during daytime (Bartoli et al., 2003; Jesus et al., 2005; MacIntyre et al., 1996). Likewise, the patchy distribution of macrofauna and its activity peak near sunset (Wenzhofer and Glud, 2004) may be responsible for enhanced heterogeneity in the oxygen distribution in the bottom currents and ensuing larger differences between the parallel-measured fluxes at sunset. Figure 3B-F show the effects of the corrections that were equally applied to optode P and Q data sets to account for changes 185 in environmental parameters and time lag error when calculating the respective fluxes. During the first 4 hours of the deployment, the raw, unprocessed cumulative fluxes (no corrections applied) derived from both optode signals were nearly identical before differences increased (Fig. 3B). Correction for temporal change in the average water oxygen concentration (Fig. 3C), led to slight rate increases in the cumulative fluxes during the day as well as during the night. The correction for time lag between current flow and oxygen signal had an effect mostly during the last 7 h of the deployment (Fig. 3D), possibly 190 due to a minor growth of biofilm on the optodes. Correction for wave rotation caused a small rate increase in fluxes, which was more pronounced during nighttime (Fig. 3E). Simultaneous application of the above corrections resulted in a nearly perfect agreement between the cumulative fluxes calculated from the two optode signals (Fig. 3F).



The parallel optode measurements confirmed short-term changes, e.g. the concentration step in the oxygen record at 18:14, 195 caused by the change of the tide (high tide: 18:16) and associated change in flow direction. The slower Seaguard oxygen sensor did not pick up this abrupt step. The temporarily increased benthic oxygen consumption near 20:00, coinciding with sunset, may have resulted from decomposition of highly degradable photosynthesis products accumulating in the sediment during daytime (Koopmans et al., 2020) and the aforementioned activity burst of the macrofauna at sunset (Wenzhofer and Glud, 2004). The parallel measurements also confirmed transient flux changes, e.g. a ~30 minute period of reduced light after 14:00 200 temporarily lowered fluxes by  $\sim 45 \text{ mmol m}^{-2} \text{ d}^{-1}$ . The ~90 minute  $\text{O}_2$  concentration and flux dip at 2:45 – 4:15 was caused by a reversing shift in the main flow direction ( $48^\circ \rightarrow 71^\circ \rightarrow 47^\circ$ ), which changed the origin of the water reaching the sensors and thereby the footprint area interrogated by the instrument (Berg et al., 2007). A correlation between 15 min  $\text{O}_2$  fluxes and average water  $\text{O}_2$  concentration changes (up to  $-0.16 \text{ mmol m}^{-2} \text{ h}^{-1}/\text{mmol l}^{-1} \text{ h}^{-1}$ ) supported that transient  $\text{O}_2$  changes had to be 205 corrected for when calculating the benthic flux. A weak correlation between 15 min  $\text{O}_2$  fluxes and short-term mean current flow changes ( $-0.03 \text{ mmol m}^{-2} \text{ h}^{-1}/\text{cm s}^{-1} \text{ h}^{-1}$ ) indicated that transient current changes had a relatively small effect on the calculated flux.

The 2OEC allows detection of compromised flux data. During the deployment in April 2014, bottom currents were higher compared to the August 16-17, 2013 deployment, averaging  $8.4 \pm 2.8 \text{ cm s}^{-1}$  with sustained peak velocities reaching  $16 \text{ cm s}^{-1}$  210 (Fig. 4A). In this deployment, the Seaguard instrument was installed at a greater distance ( $\sim 10 \text{ m}$ ) from the eddy covariance instrument, resulting in larger discrepancies between the signals of the fiber optodes and the planar optode of the Seaguard instrument, nevertheless the Seaguard data confirmed the magnitude and main trends of the fiber optode  $\text{O}_2$  concentrations 215 (Fig. 4B). Four hours into the deployment, the signals of optode P started to deviate from those of optode Q, culminating in maximum differences in the respective 15-min fluxes at 17:00-17:15 (Fig. 4C, D). A comparison of the cumulative spectra for that period (Fig. 5) indicated that the P optode may have been compromised through attachment of a marine snow particle 220 containing  $\text{O}_2$ -producing organisms. The steeper increase of the P optode 17:00 curve (Fig. 5) at the dominant wave frequency (0.2-0.3 Hz), suggested that wave orbital motion enhanced the flux, possibly by producing oscillating movement of the particle attached to the sensor tip. Past 18:00, the cumulative fluxes based on P and Q signals agreed again (Fig. 4E), suggesting that the particle was washed off the sensor. After excluding the compromised data collected between 14:00 and 18:00, the fluxes 225 calculated based on the two optode signals agreed well (daytime (P):  $3.4 \pm 0.6 \text{ mmol m}^{-2} \text{ h}^{-1}$ ,  $3.3 \pm 0.3 \text{ mmol m}^{-2} \text{ h}^{-1}$ (Q), nighttime  $-0.9 \pm 0.1 \text{ mmol m}^{-2} \text{ h}^{-1}$  (P),  $-0.9 \pm 0.7 \text{ mmol m}^{-2} \text{ h}^{-1}$  (Q); daytime average  $3.3 \pm 0.7 \text{ mmol m}^{-2} \text{ h}^{-1}$  (P, Q), nighttime average  $-0.9 \pm 0.7 \text{ mmol m}^{-2} \text{ h}^{-1}$  (P, Q)).

The 2OEC can reduce data loss as exemplified by the 14-15 August 2013 deployment (Fig. 6). Although the oxygen 225 concentrations recorded by the 2OEC and the Seaguard optodes agreed during the deployment (Fig. 6B), optode P was compromised over extended time periods likely due to a particle caught by the sensor. After almost identical fluxes during the first hour (P:  $4.0 \pm 0.4 \text{ mmol m}^{-2} \text{ h}^{-1}$ , Q:  $4.1 \pm 0.3 \text{ mmol m}^{-2} \text{ h}^{-1}$ , Fig. 6E), the cumulative optode P flux decreased relative to



the optode Q based flux, despite ongoing benthic photosynthetic oxygen production. This decline in P cumulative flux levelled out at 20:00 and remained steady until 22:00 before the trajectories of the two cumulative fluxes matched again. The following 230 good agreement between P and Q cumulative fluxes between 22:00-5:00 (P:  $-3.5 \pm 0.1 \text{ mmol m}^{-2} \text{ h}^{-1}$ , Q:  $-3.6 \pm 0.3 \text{ mmol m}^{-2} \text{ h}^{-1}$ , Fig. 6E) indicated that sensor P resumed normal operation. Such a sensor recovery can be observed when water currents remove particles that had attached to the sensor disturbing its signal. The identification of the drop in cumulative P flux as an artefact was supported by the comparison with sensor Q, which produced the typical circadian cumulative flux pattern with a steady increase during the light phase until sunset and decrease thereafter throughout the dark phase. After 5:00, still during 235 dark conditions, the increase in cumulative P flux and divergence from the cumulative Q flux suggested that sensor P then lost its calibration, which occurs when the sensor loses some of the dye coating that produces the signal (e.g. through particle impact). The temporary good agreement of the cumulative fluxes based on P and Q optode readings permitted salvaging sections of the flux record and thereby allowed at least rough estimates for day and nighttime fluxes for this deployment. The parallel chamber deployments supported these estimates (daytime:  $4.3 \pm 2.6 \text{ mmol m}^{-2} \text{ h}^{-1}$ , nighttime:  $-3.2 \pm 0.6 \text{ mmol m}^{-2} \text{ h}^{-1}$ , 240 Fig. 7D).

### 3.2 Differences between P and Q fluxes and comparison with advection chamber fluxes

After exclusion of flux intervals compromised by biofouling, the differences between P and Q optode fluxes derived from the slopes of the cumulative flux curves (Figs. 2E, 4E, 6E) averaged 2.3%, -0.1% and -4.7% during daytime and 1.7%, 16.2% and 245 -3.2% during nighttime, for the three deployments respectively. These agreements within < 20% strengthened the flux estimates. Fluxes determined with the 2OEC further were supported by the fluxes measured with the advection chambers conducted parallel to the eddy covariance measurement during the August 2013 deployments (Fig. 7). The average chamber daytime fluxes for the two deployments ( $3.9 \pm 3.0 \text{ mmol m}^{-2} \text{ h}^{-1}$ ) were similar to the respective eddy covariance fluxes ( $3.7 \pm 0.9 \text{ mmol m}^{-2} \text{ h}^{-1}$ ) (Fig 7C), although the chamber nighttime fluxes ( $-3.4 \pm 0.8 \text{ mmol m}^{-2} \text{ h}^{-1}$ ) exceeded those of the eddy 250 covariance instrument ( $-2.5 \pm 1.3 \text{ mmol m}^{-2} \text{ h}^{-1}$ ) by factor 1.4 (Fig 7C). This difference was caused by the smaller nighttime fluxes recorded by the 2OEC during the second August 2013 deployment (Fig 7B). The chambers measured flux over the same enclosed sediment area over the duration of the deployment, while the footprint of the eddy measurements moved with current direction, which may explain the differences in dark fluxes observed between 2OEC and chambers during the 16-17 Aug 2013 deployment (Fig. 7 B). The differences between average eddy and average chamber fluxes were statistically not significant 255 (Fig 7C).

## 4 Discussion

The small and rapid changes in concentration and flow the aquatic eddy covariance instrumentation must record for accurate flux determination make the technique sensitive to even small disturbances affecting the measuring process (Reimers et al.,



2012b). By using two solute sensors recording in parallel, the 2OEC allows detection of measuring artefacts and thereby can  
260 enhance the reliability of the flux determinations. The general functionality of the 2OEC and the ranges of fluxes it recorded  
were supported by the advection chamber fluxes measured parallel to the eddy flux recordings.

The 2OEC improves detection of sensor fouling. This is significant as the most common and most unnoticed cause for  
aquatic eddy covariance measuring errors likely is the attachment of marine snow particles or biofilms to the solute sensor.  
Through physical separation of the sensing surface from the water, such fouling increases sensor response time, which  
265 decreases the measured rates of oxygen change and the temporal alignment of oxygen and flow data. Furthermore, biological  
and chemical reactions in such organic coatings can produce or consume oxygen and thereby compromise flux calculations.  
As the growth of a biofilm on the sensor may be gradual, the detection of the onset of flux bias caused by biofouling may be  
impossible in a single-sensor instrument. A very good agreement of the cumulative fluxes calculated from the two 2OEC  
270 optodes as in the 16-17 August 2013 deployment is a strong indication that the sensors worked correctly (Fig. 2), while  
differences between the cumulative fluxes as in the 14-15 August 2013 deployment are indicative of sensor malfunction  
(Fig. 6E).

The comparison of the cumulative fluxes can reveal even short or small deviations of the sensor signal as e.g. caused by a  
temporary attachment of a marine snow particle (Fig. 4E). During the 10-11 Apr 2014 deployment, unusual contributions to  
optode P fluxes in the wave frequency band (0.2 to 0.3 Hz) that were not mirrored in optode Q, identified optode P as  
275 compromised starting at 15:00 for a ~3 h duration (Fig. 5). A marine snow particle with photosynthesizing organisms  
attached to the tip of the oxygen sensor and moved by wave orbital motion can synchronize vertical current flow oscillations  
and the effect of the particle on the oxygen reading (e.g. increased oxygen due to photosynthesis) and thereby lead to  
erroneous flux estimates. In single sensor eddy covariance instruments, obvious temporary sensor malfunctions typically flag  
long sections or the entire deployment as compromised because it is difficult to determine with certainty when and for how  
280 long the sensor reading has been biased. The relatively frequent occurrence of sensor fouling therefore causes substantial  
losses in data, time and costs. The dual sensor approach can reduce such losses because it allows identifying periods of  
unbiased measurements within partly compromised data records.

The reliability of the flux data hinges on unbiased sensor data that can capture temporal variability of current flow and the  
oxygen it carries, which may change as rapidly as 1-3 Hz (Kuwae et al., 2006; McGinnis et al., 2008a). The ADV used in the  
285 2OEC can produce calibrated current data non-invasively at a frequency of 64 Hz, while the fiber optode has a slower  
response time (200-300 ms, (Merikhi et al., 2018)), and its placement near the ADV measuring volume may affect current  
flow measurements and thereby could bias the flux calculations. The Pyroscience fiber optode used with the 2OEC is one of  
the smallest and fastest oxygen sensors available, and a comparison with the most common oxygen sensors presently utilized  
for aquatic eddy covariance (Table A4) favors the selection of this sensor for many field settings. For this comparison, three



290 eddy covariance instruments equipped with either (1) one Unisense electrochemical microelectrode (Berg et al., 2019), (2) one JFE Advantech Rinko planar optode (Berg et al., 2016), or (3) one Pyroscience fiber optode were deployed side by side (i.e. 10 m spacing) at our study site 3-4 December 2016. All instruments used the same type of tripod and ADV and the oxygen sensors were mounted at a 45-degree downward angle as described for the 2OEC. The three different sensors measured very similar fluxes when the current flow approached the sensor tips from the front as shown in Fig. 8A, burst 11  
295 to 28. This changed when the flow approached the sensors from the back. The RINKO sensor under such flow conditions may self-shade its planar optode, which may result in an underestimation of the fluxes at higher frequencies (0.1-1.0 Hz, Fig. 8B) as seen in burst 1 to 9 (Fig. 8A), and possibly also disturb the flow in the Vector flow measuring volume. There were no significant differences between the fluxes based on the fiber optode and the microelectrode for the reversed flow, supporting the choice of the sturdier fiber optodes for oxygen measurements with aquatic eddy covariance instruments.

300 **5 Conclusions**

The advantages of 2OEC flux measurements over invasive measurements (e.g. benthic chambers) may be most significant for deployments in continental margins. The dynamic nature and magnitudes of the benthic processes increase with decreasing water depth, with benthic fluxes reaching highest rates in the shelf environment (Huettel et al., 2014; Middelburg and Soetaert, 2004; Jahnke, 2010; Bauer et al., 2013; Reimers et al., 2004). Here light and bottom currents may strongly  
305 influence benthic fluxes (Gattuso et al., 2006). The relatively high fluxes and daytime benthic oxygen release recorded at our oligotrophic sandy study site, supported by flux measurements from similar subtropical and tropical carbonate environments (Bednarz et al., 2015; Rao et al., 2012; Wild et al., 2009; Wild et al., 2005; Glud et al., 2008), emphasize the need for instrumentation that reliably can take light and currents at the seafloor into account when measuring benthic fluxes. The 2OEC is a powerful tool that meets these requirements, and its relatively high temporal resolution can provide new insights  
310 into the dynamics of benthic oxygen flux.



320 **6 Appendix A**

**Table A1: Specifications of the Pyroscience™ FireStingO<sub>2</sub>-Mini oxygen meter**

Pyroscience™ FireStingO <sub>2</sub> -Mini	Single sensor module,
Oxygen port	1 fiber-optic ST-connector
Temperature port	4-wire PT100, -30°C-150°C, 0.02°C resolution, ±0.5°C accuracy
Dimensions and Weight	67 x 25 x 25 mm, 70 g
Measuring principle	Luminescence lifetime detection (REDFLASH)
Excitation Wavelength	620 nm (orange-red)
Emission wavelength	760 nm (NIR)
Maximum sampling rate	20 Hz
Interface	Serial interface (UART), ASCII communication protocol
Analog output	0 - 2.5 V DC, 14 bit resolution
Power requirements	Max. 70 mA at 5 V DC from USB (typ. 50 mA)

**Table A2: Specifications of the Pyroscience™ OXR430-UHS retractable oxygen minisensors**

Optical O <sub>2</sub> fiber sensor type	Pyroscience™ OXR430-UHS
Fiber diameter	430 µm
Optimal measuring range	0-720 µmol l <sup>-1</sup>
Maximum measuring range	0 - 1440 µmol l <sup>-1</sup>
Response time	< 0.3 s
Detection limit	0.3 µmol l <sup>-1</sup>
Resolution at 1% O <sub>2</sub>	0.16 µmol l <sup>-1</sup>
Resolution at 20% O <sub>2</sub>	0.78 µmol l <sup>-1</sup>
Accuracy at 1% O <sub>2</sub>	± 0.31 µmol l <sup>-1</sup>
Accuracy at 20% O <sub>2</sub>	± 3.13 µmol l <sup>-1</sup>
Temperature range	0 - 50°C

325 **Table A3: Specifications of the NORTEK Vector acoustic Doppler velocimeter**

Sensor	Range	Accuracy	Precision/Resolution
Velocity	±0.01, 0.1, 0.3, 1, 2, 4, 7 m s <sup>-1</sup>	± 0.5%	± 1%
Pressure	0-20 m (shallow water version)	0.5% (full scale)	< 0.005% of full scale
Temperature	-4 to +40 °C	0.1 °C	0.01 °C
Compass	360°	2°	0.1°
Tilt	< 30°	0.2°	0.1°

**Table A4. The specifications of the oxygen microelectrode, Rinko planar optode and Pyroscience fiber optode**

Sensor	OX-10 fast (µm)	RINKO EC	OXR430-UHS
Type	Microelectrode	Planar optode	Fiber optode
Manufacturer	Unisense	JFE-Advantech	Pyroscience
Measurement principle	Electrolytical reduction	Phosphorescence	Phosphorescence
Tip diameter (µm)	10	12000	430
Response time (90%) (s)	< 0.3	< 0.5	< 0.3
Range (% air saturation)	0-200	0-200	0-500



330 **7 Data availability**

The current flow and oxygen data collected with the 2OEC during the August 2013 and April 2014 deployments were submitted to the Biological and Chemical Oceanography Data Management Office (BCO-DMO, <https://www.bco-dmo.org/>).

**8 Author contributions**

MH designed and assembled the 2OEC instrument, MH, PB and AM deployed the 2OEC, and analyzed the data. MH prepared  
335 the manuscript with contributions from all co-authors.

**9 Competing interest statement**

The authors declare that they have no conflict of interest.

**10 Acknowledgments**

We thank the staff of the FIO Florida Keys Marine Laboratory for help with instrument deployments and sample collection.  
340 The research was conducted under NOAA permit FKNMS-2012-137-A2 and was supported by NSF grants OCE-1334117 and OCE-1851290.



## 11 References

Attard, K. M., Rodil, I. F., Glud, R. N., Berg, P., Norkko, J., and Norkko, A.: Seasonal ecosystem metabolism across shallow benthic habitats measured by aquatic eddy covariance, *Limnology and Oceanography Letters*, 4, 79-86, 10.1002/lol2.10107, 2019.

Bartoli, M., Nizzoli, D., and Viaroli, P.: Microphytobenthos activity and fluxes at the sediment-water interface: interactions and spatial variability, *Aquatic Ecology*, 37, 341-349, 10.1023/B:AECO.0000007040.43077.5f, 2003.

Bauer, J. E., Cai, W.-J., Raymond, P. A., Bianchi, T. S., Hopkinson, C. S., and Regnier, P. A. G.: The changing carbon cycle of the coastal ocean, *Nature*, 504, 61-70, 10.1038/nature12857, 2013.

Bednarz, V. N., van Hoytema, N., Cardini, U., Naumann, M. S., Al-Rshaidat, M. M. D., and Wild, C.: Dinitrogen fixation and primary productivity by carbonate and silicate reef sand communities of the Northern Red Sea, *Marine Ecology Progress Series*, 527, 47-57, 10.3354/meps11224, 2015.

Berg, P., Roy, H., Janssen, F., Meyer, V., Jorgensen, B. B., Huettel, M., and de Beer, D.: Oxygen uptake by aquatic sediments measured with a novel non-invasive eddy-correlation technique, *Marine Ecology-Progress Series*, 261, 75-83, 2003.

Berg, P., Roy, H., and Wiberg, P. L.: Eddy correlation flux measurements: The sediment surface area that contributes to the flux, *Limnology and Oceanography*, 52, 1672-1684, 2007.

Berg, P., Glud, R. N., Hume, A., Stahl, H., Oguri, K., Meyer, V., and Kitazato, H.: Eddy correlation measurements of oxygen uptake in deep ocean sediments, *Limnology and Oceanography-Methods*, 7, 576-584, 10.4319/lom.2009.7.576, 2009.

Berg, P., Long, M. H., Huettel, M., Rheuban, J. E., McGlathery, K. J., Howarth, R. W., Foreman, K. H., Giblin, A. E., and Marino, R.: Eddy correlation measurements of oxygen fluxes in permeable sediments exposed to varying current flow and light, *Limnology and Oceanography*, 58, 1329-1343, 10.4319/lo.2013.58.4.1329, 2013.

Berg, P., Reimers, C. E., Rosman, J. H., Huettel, M., Delgard, M. L., Reidenbach, M. A., and Ozkan-Haller, H. T.: Technical note: Time lag correction of aquatic eddy covariance data measured in the presence of waves, *Biogeosciences*, 12, 6721-6735, 10.5194/bg-12-6721-2015, 2015.

Berg, P., Koopmans, D. J., Huettel, M., Li, H., Mori, K., and Wuest, A.: A new robust oxygen-temperature sensor for aquatic eddy covariance measurements, *Limnology and Oceanography-Methods*, 14, 151-167, 10.1002/lom3.10071, 2016.

Berg, P., Delgard, M. L., Reimers, C., Glud, R., Huettel, M., and Pace, M.: Non-invasive Flux Measurements at the Benthic Interface: the Aquatic Eddy Covariance Technique. ASLO, ASLO e-Lectures, 2017.

Berg, P., and Pace, M. L.: Continuous measurement of air-water gas exchange by underwater eddy covariance, *Biogeosciences*, 14, 5595-5606, 10.5194/bg-14-5595-2017, 2017.



375 Berg, P., Delgard, M. L., Polsenaere, P., McGlathery, K. J., Doney, S. C., and Berger, A. C.: Dynamics of benthic metabolism, O<sub>2</sub>, and pCO<sub>2</sub> in a temperate seagrass meadow, *Limnology and Oceanography*, 64, 2586-2604, 10.1002/lno.11236, 2019.

Berger, A. C., Berg, P., McGlathery, K. J., and Delgard, M. L.: Long-term trends and resilience of seagrass metabolism: A decadal aquatic eddy covariance study, *Limnology and Oceanography*, 10.1002/lno.11397, 2020.

380 Bittig, H. C., Kortzinger, A., Neill, C., van Ooijen, E., Plant, J. N., Hahn, J., Johnson, K. S., Yang, B., and Emerson, S. R.: Oxygen Optode Sensors: Principle, Characterization, Calibration, and Application in the Ocean, *Frontiers in Marine Science*, 4, 10.3389/fmars.2017.00429, 2018.

Brand, A., McGinnis, D. F., Wehrli, B., and Wueest, A.: Intermittent oxygen flux from the interior into the bottom boundary of lakes as observed by eddy correlation, *Limnology and Oceanography*, 53, 1997-2006, 10.4319/lo.2008.53.5.1997, 2008.

385 Chipman, L., Huettel, M., Berg, P., Meyer, V., Klimant, I., Glud, R., and Wenzhoefer, F.: Oxygen optodes as fast sensors for eddy correlation measurements in aquatic systems, *Limnology And Oceanography-Methods*, 10, 304-316, 10.4319/lom.2012.10.304, 2012.

Chipman, L., Berg, P., and Huettel, M.: Benthic Oxygen Fluxes Measured by Eddy Covariance in Permeable Gulf of Mexico Shallow-Water Sands, *Aquatic Geochemistry*, 22, 529-554, 10.1007/s10498-016-9305-3, 2016.

Cook, P. L. M., Wenzhoefer, F., Glud, R. N., Janssen, F., and Huettel, M.: Benthic solute exchange and carbon mineralization 390 in two shallow subtidal sandy sediments: Effect of advective pore-water exchange, *Limnology and Oceanography*, 52, 1943-1963, 2007.

Crusius, J., Berg, P., Koopmans, D. J., and Erban, L.: Eddy correlation measurements of submarine groundwater discharge, *Marine Chemistry*, 109, 77-85, 10.1016/j.marchem.2007.12.004, 2008.

395 Cyronak, T., Santos, I. R., McMahon, A., and Eyre, B. D.: Carbon cycling hysteresis in permeable carbonate sands over a diel cycle: Implications for ocean acidification, *Limnology and Oceanography*, 58, 131-143, 10.4319/lo.2013.58.1.0131, 2013.

DeBeer, D., Wenzhoefer, F., Ferdelman, T. G., Boehme, S. E., Huettel, M., van Beusekom, J. E. E., Bottcher, M. E., Musat, N., and Dubilier, N.: Transport and mineralization rates in North Sea sandy intertidal sediments, Sylt-Romo Basin, Wadden Sea, *Limnology and Oceanography*, 50, 113-127, 2005.

400 Delauney, L., Compere, C., and Lehaire, M.: Biofouling protection for marine environmental sensors, *Ocean Science*, 6, 503-511, 10.5194/os-6-503-2010, 2010.

Donis, D., Holtappels, M., Noss, C., Cathalot, C., Hancke, K., Polsenaere, P., Wenzhoefer, F., Lorke, A., Meysman, F. J. R., Glud, R. N., and McGinnis, D. F.: An Assessment of the Precision and Confidence of Aquatic Eddy Correlation Measurements, *Journal of Atmospheric and Oceanic Technology*, 32, 642-655, 10.1175/jtech-d-14-00089.1, 2015.

405 Eyre, B. D., Santos, I. R., and Maher, D. T.: Seasonal, daily and diel N<sub>2</sub> effluxes in permeable carbonate sediments, *Biogeosciences*, 10, 2601-2615, 10.5194/bg-10-2601-2013, 2013.



Eyre, B. D., Cyronak, T., Drupp, P., De Carlo, E. H., Sachs, J. P., and Andersson, A. J.: Coral reefs will transition to net dissolving before end of century, *Science*, 359, 908-911, 10.1126/science.aoa1118, 2018.

Gattuso, J. P., Gentili, B., Duarte, C. M., Kleypas, J. A., Middelburg, J. J., and Antoine, D.: Light availability in the coastal ocean: impact on the distribution of benthic photosynthetic organisms and their contribution to primary production, *Biogeosciences*, 3, 489-513, 2006.

Glud, R. N.: Oxygen dynamics of marine sediments, *Marine Biology Research*, 4, 243-289, 2008.

Glud, R. N., Eyre, B. D., and Patten, N.: Biogeochemical responses to mass coral spawning at the Great Barrier Reef: Effects on respiration and primary production, *Limnology and Oceanography*, 53, 1014-1024, 2008.

Glud, R. N., Berg, P., Hume, A., Batty, P., Blacher, M. E., Lennert, K., and Rysgaard, S.: Benthic O<sub>2</sub> exchange across hard-bottom substrates quantified by eddy correlation in a sub-Arctic fjord, *Marine Ecology-Progress Series*, 417, 1-12, 10.3354/meps08795, 2010.

Glud, R. N., Berg, P., Stahl, H., Hume, A., Larsen, M., Eyre, B. D., and Cook, P. L. M.: Benthic Carbon Mineralization and Nutrient Turnover in a Scottish Sea Loch: An Integrative In Situ Study, *Aquatic Geochemistry*, 22, 443-467, 10.1007/s10498-016-9300-8, 2016.

Gundersen, J. K., Ramsing, N. B., and Glud, R. N.: Predicting the signal of O<sub>2</sub> microsensors from physical dimensions, temperature, salinity, and O<sub>2</sub> concentration, *Limnology & Oceanography*, 43, 1932-1937, 1998.

Holst, G., Kohls, O., Klimant, I., Koenig, B., Kuehl, M., and Richter, T.: A modular luminescence lifetime imaging system for mapping oxygen distribution in biological samples, *Sensors and Actuators B*, 51, 163-170, 1998.

Holtappels, M., Glud, R. N., Donis, D., Liu, B., Hume, A., Wenzhofer, F., and Kuyper, M. M. M.: Effects of transient bottom water currents and oxygen concentrations on benthic exchange rates as assessed by eddy correlation measurements, *Journal of Geophysical Research-Oceans*, 118, 1157-1169, 10.1002/jgrc.20112, 2013.

Holtappels, M., Noss, C., Hancke, K., Cathalot, C., McGinnis, D. F., Lorke, A., and Glud, R. N.: Aquatic Eddy Correlation: Quantifying the Artificial Flux Caused by Stirring-Sensitive O<sub>2</sub> Sensors, *Plos One*, 10, 10.1371/journal.pone.0116564, 2015.

Huettel, M., and Gust, G.: Solute Release Mechanisms From Confined Sediment Cores In Stirred Benthic Chambers and Flume Flows, *Marine Ecology Progress Series*, 82, 187-197, 1992.

Huettel, M., and Rusch, A.: Transport and degradation of phytoplankton in permeable sediment, *Limnology & Oceanography*, 45, 534-549, 2000.

Huettel, M., Berg, P., and Kostka, J. E.: Benthic Exchange and Biogeochemical Cycling in Permeable Sediments, *Annual Review of Marine Science*, Vol 6, 6, 23-51, 10.1146/annurev-marine-051413-012706, 2014.

Hume, A. C., Berg, P., and McGlathery, K. J.: Dissolved oxygen fluxes and ecosystem metabolism in an eelgrass (*Zostera marina*) meadow measured with the eddy correlation technique, *Limnology and Oceanography*, 56, 86-96, 10.4319/lo.2011.56.1.0086, 2011.



440 Jahnke, R.: Global Synthesis, in: Carbon and Nutrient Fluxes in Continental Margins, edited by: Liu, K. K., Atkinson, L. P., Quinones, R., and Talaure-McManus, L., Springer, 597–615, 2010.

Janssen, F., Faerber, P., Huettel, M., Meyer, V., and Witte, U.: Pore-water advection and solute fluxes in permeable marine sediments (I): Calibration and performance of the novel benthic chamber system Sandy, Limnology and Oceanography, 50, 768-778, 2005a.

445 Janssen, F., Huettel, M., and Witte, U.: Pore-water advection and solute fluxes in permeable marine sediments (II): Benthic respiration at three sandy sites with different permeabilities (German Bight, North Sea), Limnology and Oceanography, 50, 779-792, 2005b.

Jesus, B., Brotas, V., Marani, M., and Paterson, D. M.: Spatial dynamics of microphytobenthos determined by PAM fluorescence, Estuarine Coastal and Shelf Science, 65, 30-42, 10.1016/j.ecss.2005.05.005, 2005.

450 Johnson, K. S., Chavez, F. P., and Friederich, G. E.: Continental-shelf sediment as a primary source of iron for coastal phytoplankton, Nature, 398, 697-700, 1999.

Klimant, I., Meyer, V., and Kuehl, M.: Fiber-optic oxygen microsensors, a new tool in aquatic biology, Limnology and Oceanography, 40, 1159-1165, 1995.

Koopmans, D., Holtappels, M., Chennu, A., Weber, M., and de Beer, D.: High Net Primary Production of Mediterranean 455 Seagrass (*Posidonia oceanica*) Meadows Determined With Aquatic Eddy Covariance, Frontiers in Marine Science, 7, 10.3389/fmars.2020.00118, 2020.

Kuwae, T., Kamio, K., Inoue, T., Miyoshi, E., and Uchiyama, Y.: Oxygen exchange flux between sediment and water in an intertidal sandflat, measured in situ by the eddy-correlation method, Marine Ecology Progress Series, 307, 59-68, 10.3354/meps307059, 2006.

460 Lehner, P., Staudinger, C., Borisov, S. M., Regensburger, J., and Klimant, I.: Intrinsic Artefacts in Optical Oxygen Sensors- How Reliable are our Measurements?, Chemistry-a European Journal, 21, 3978-3986, 10.1002/chem.201406037, 2015.

Long, M. H., Koopmans, D., Berg, P., Rysgaard, S., Glud, R. N., and Sogaard, D. H.: Oxygen exchange and ice melt measured at the ice-water interface by eddy correlation, Biogeosciences, 9, 1957-1967, 10.5194/bg-9-1957-2012, 2012.

465 Long, M. H., Berg, P., de Beer, D., and Zieman, J. C.: In Situ Coral Reef Oxygen Metabolism: An Eddy Correlation Study, Plos One, 8, 10.1371/journal.pone.0058581, 2013.

Lorrai, C., McGinnis, D. F., Berg, P., Brand, A., and Wuest, A.: Application of Oxygen Eddy Correlation in Aquatic Systems, Journal of Atmospheric and Oceanic Technology, 27, 1533-1546, 10.1175/2010jtecho723.1, 2010.

MacIntyre, H. L., Geider, R. J., and Miller, D. C.: Microphytobenthos: The ecological role of the "secret garden" of unvegetated, shallow-water marine habitats .1. Distribution, abundance and primary production, Estuaries, 19, 186-201, 470 10.2307/1352224, 1996.

McGinnis, D. F., Berg, P., Brand, A., Lorrai, C., Edmonds, T. J., and Wuest, A.: Measurements of eddy correlation oxygen fluxes in shallow freshwaters: Towards routine applications and analysis, Geophysical Research Letters, 35, 10.1029/2007gl032747, 2008a.



McGinnis, D. F., Berg, P., Brand, A., Lorrai, C., Edmonds, T. J., and Wuest, A.: Measurements of eddy correlation oxygen fluxes in shallow freshwaters: Towards routine applications and analysis, *Geophysical Research Letters*, 35, 10.1029/2007gl032747, 2008b.

McGinnis, D. F., Sommer, S., Lorke, A., Glud, R. N., and Linke, P.: Quantifying tidally driven benthic oxygen exchange across permeable sediments: An aquatic eddy correlation study, *Journal of Geophysical Research-Oceans*, 119, 6918-6932, 10.1002/2014jc010303, 2014.

Merikhi, A., Berg, P., Meyer, V., and Huettel, M.: Jet-nozzle method for measuring response times of scalar sensors used in liquids and gases, *Limnology and Oceanography-Methods*, 16, 475-483, 10.1002/lom3.10259, 2018.

Middelburg, J. J., and Soetaert, K.: The role of sediments in shelf ecosystem dynamics, *Geochimica et Cosmochimica Acta*, 68, A343-A343, 2004.

Navarro-Villoslada, F., Orellana, G., Moreno-Bondi, M. C., Vick, T., Driver, M., Hildebrand, G., and Liefeth, K.: Fiber-optic luminescent sensors with composite oxygen-sensitive layers and anti-biofouling coatings, *Analytical Chemistry*, 73, 5150-5156, 10.1021/ac015517n, 2001.

Rao, A. M. F., Polerecky, L., Ionescu, D., Meysman, F. J. R., and de Beer, D.: The influence of pore-water advection, benthic photosynthesis, and respiration on calcium carbonate dynamics in reef sands, *Limnology and Oceanography*, 57, 809-825, 10.4319/lo.2012.57.3.0809, 2012.

Reimers, C. E., Stecher III, H. A., Taghon, G. L., Fuller, C. M., Huettel, M., Rusch, A., Ryckelynck, N., and Wild, C.: In situ measurements of advective solute transport in permeable shelf sands, *Continental Shelf Research*, 24, 183–201, 2004.

Reimers, C. E., Oezkan-Haller, H. T., Berg, P., Devol, A., McCann-Grosvenor, K., and Sanders, R. D.: Benthic oxygen consumption rates during hypoxic conditions on the Oregon continental shelf: Evaluation of the eddy correlation method, *Journal of Geophysical Research-Oceans*, 117, 10.1029/2011jc007564, 2012a.

Reimers, C. E., Ozkan-Haller, H. T., Berg, P., Devol, A., McCann-Grosvenor, K., and Sanders, R. D.: Benthic oxygen consumption rates during hypoxic conditions on the Oregon continental shelf: Evaluation of the eddy correlation method, *Journal of Geophysical Research-Oceans*, 117, 10.1029/2011jc007564, 2012b.

Rheuban, J. E., Berg, P., and McGlathery, K. J.: Ecosystem metabolism along a colonization gradient of eelgrass (*Zostera marina*) measured by eddy correlation, *Limnology and Oceanography*, 59, 1376-1387, 10.4319/lo.2014.59.4.1376, 2014a.

Rheuban, J. E., Berg, P., and McGlathery, K. J.: Multiple timescale processes drive ecosystem metabolism in eelgrass (*Zostera marina*) meadows, *Marine Ecology Progress Series*, 507, 1-13, 10.3354/meps10843, 2014b.

Rodil, I. F., Attard, K. M., Norkko, J., Glud, R. N., and Norkko, A.: Towards a sampling design for characterizing habitat-specific benthic biodiversity related to oxygen flux dynamics using Aquatic Eddy Covariance, *Plos One*, 14, 10.1371/journal.pone.0211673, 2019.

Santos, I. R., Glud, R. N., Maher, D., Erler, D., and Eyre, B. D.: Diel coral reef acidification driven by porewater advection in permeable carbonate sands, Heron Island, Great Barrier Reef, *Geophysical Research Letters*, 38, 10.1029/2010gl046053, 2011.



Smith, M. J., Kerr, A., and Cowling, M. J.: Effects of marine biofouling on gas sensor membrane materials, *Journal of Environmental Monitoring*, 9, 1378-1386, 10.1039/b714187b, 2007.

510 Stern, O., and Volmer, M.: The fading time of fluorescence, *Physikalische Zeitschrift*, 20, 183-188, 1919.

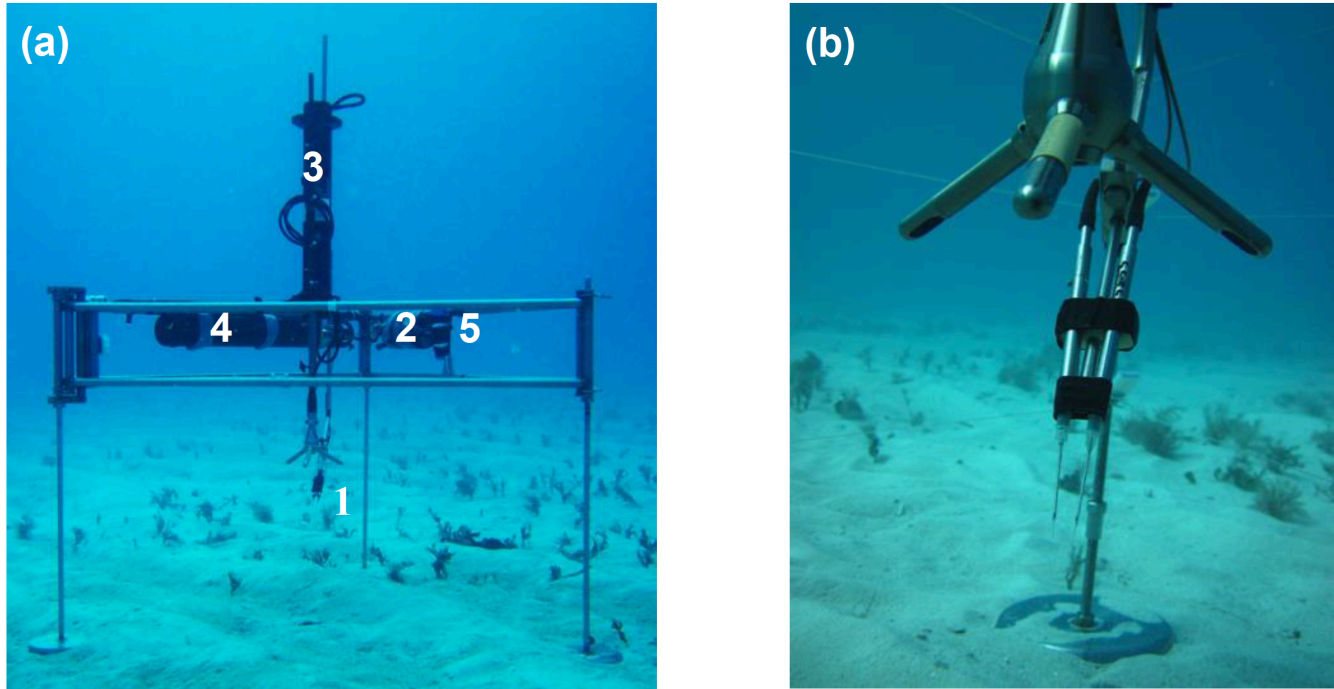
Walsh, J. J.: On the nature of continental shelves, Academic Press, New York, 520 pp., 1988.

Wang, X. D., and Wolfbeis, O. S.: Optical methods for sensing and imaging oxygen: materials, spectroscopies and applications, *Chemical Society Reviews*, 43, 3666-3761, 10.1039/c4cs00039k, 2014.

515 Wenzhofer, F., and Glud, R. N.: Small-scale spatial and temporal variability in coastal benthic O<sub>2</sub> dynamics: Effects of fauna activity, *Limnology and Oceanography*, 49, 1471-1481, 2004.

Wild, C., Rasheed, M., Jantzen, C., Cook, P., Struck, U., Huettel, M., and Boetius, A.: Benthic metabolism and degradation of natural particulate organic matter in carbonate and silicate reef sands of the northern Red Sea, *Marine Ecology-Progress Series*, 298, 69-78, 2005.

520 Wild, C., Naumann, M. S., Haas, A., Struck, U., Mayer, F. W., Rasheed, M. Y., and Huettel, M.: Coral sand O<sub>2</sub> uptake and pelagic-benthic coupling in a subtropical fringing reef, Aqaba, Red Sea, *Aquatic Biology*, 6, 133-142, 10.3354/ab00181, 2009.



525  
**Figure 1: (A) The eddy covariance instrument with dual fiber optode sensor at the study site. The tripod carries the optodes (1), underwater housing with oxygen meters reading the optodes (2), acoustic Doppler Velocimeter (ADV) (3) battery pack (4) and light logger (5) (B) Close up of the dual optode sensors.**

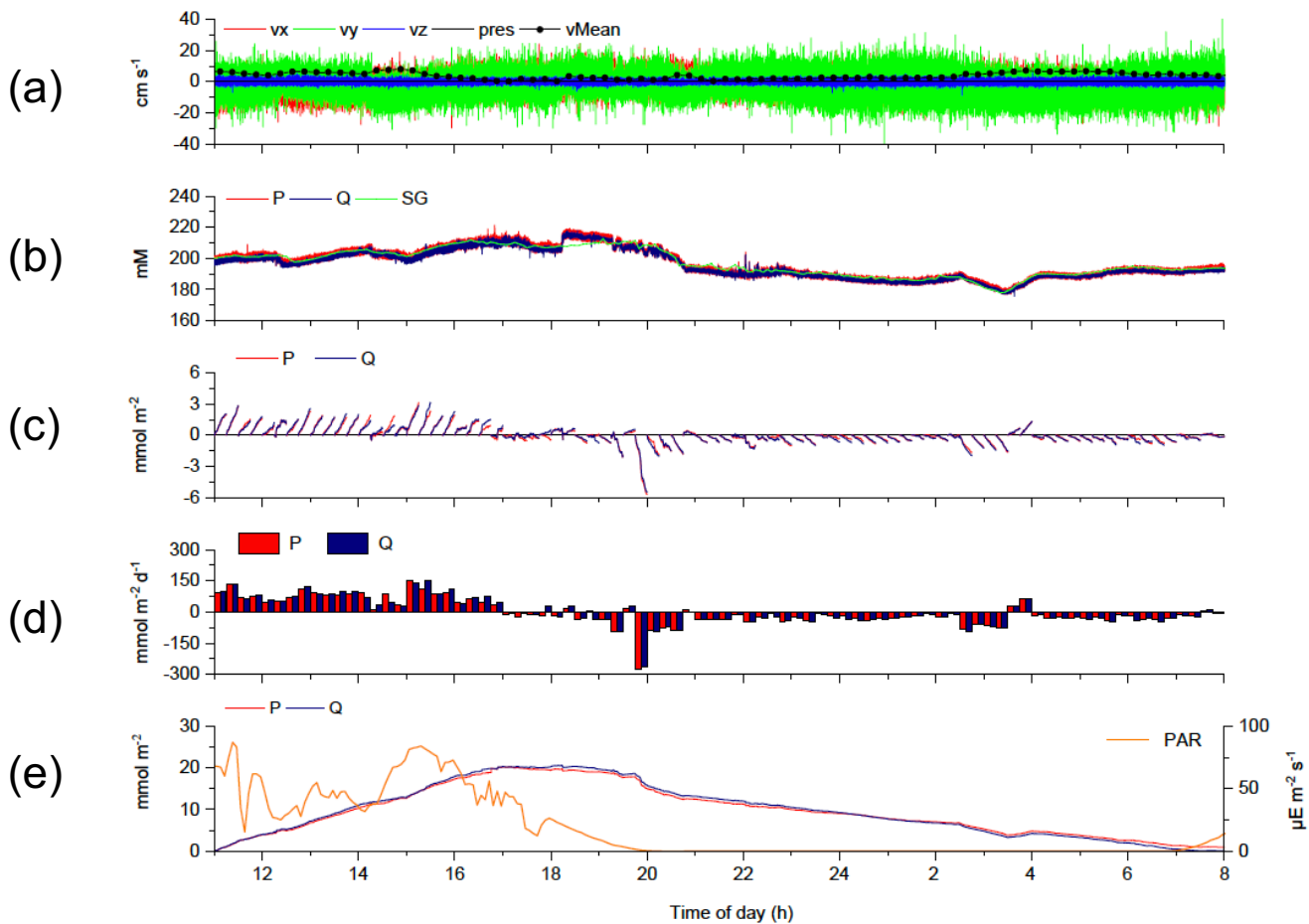
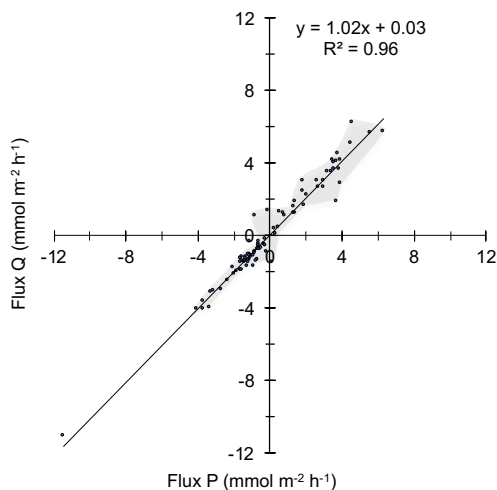


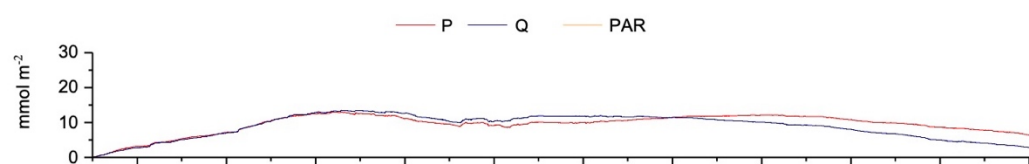
Figure 2: (A) 2OEC deployment of 16-17 August 2013. A) horizontal x (red), y (green), and vertical z (blue) bottom flow components and mean current velocity (black circles). B) Oxygen concentrations measured by the two optodes P (red) and Q (blue) and the Seaguard planar optode (green). C) time-lag, rotation and storage corrected cumulative fluxes plotted for 15 min intervals. D) average 15 min fluxes, E) cumulative fluxes and PAR light intensity at the seafloor (orange line). Graphs produced with software Origin<sup>®</sup> 2017 (OriginLab).



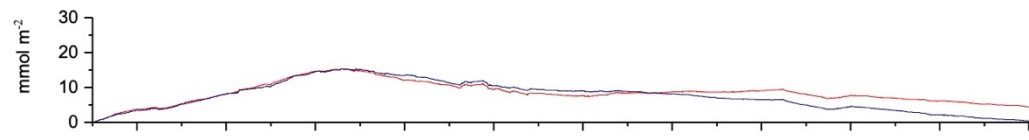
(a)



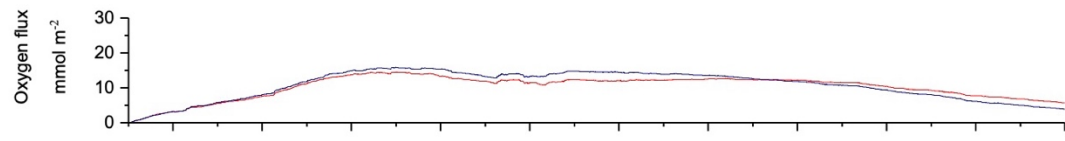
(b)



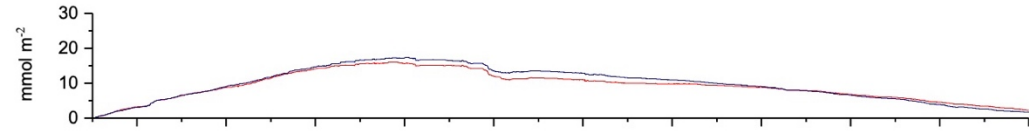
(c)



(d)



(e)



(f)

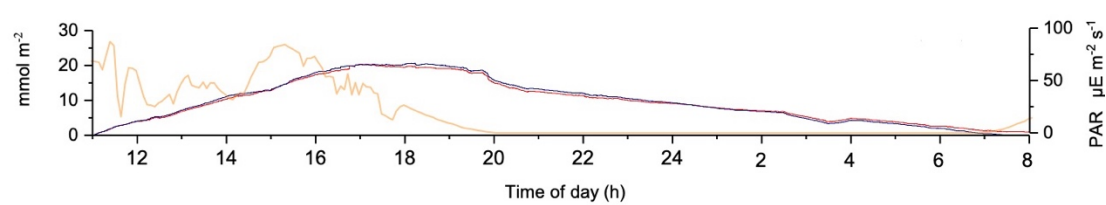
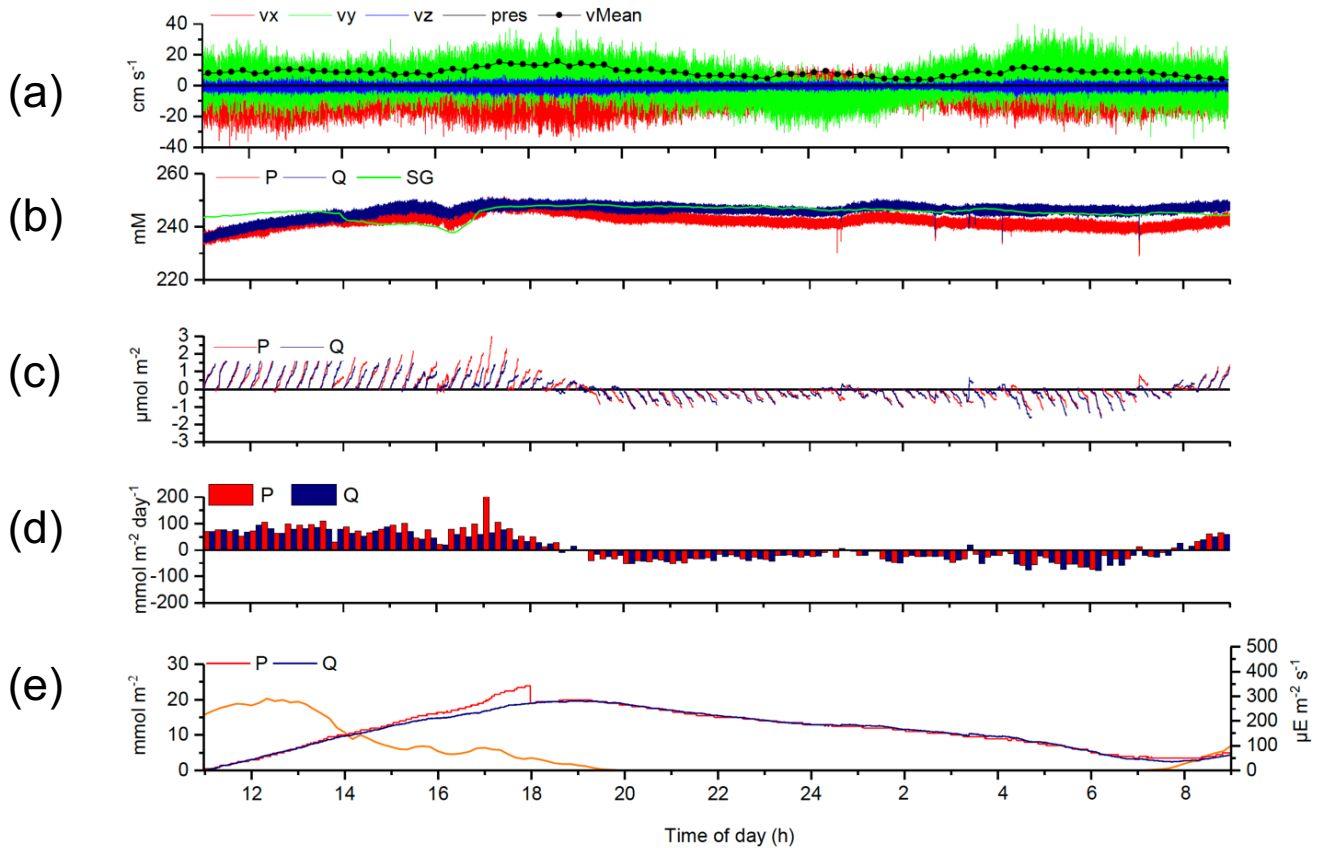
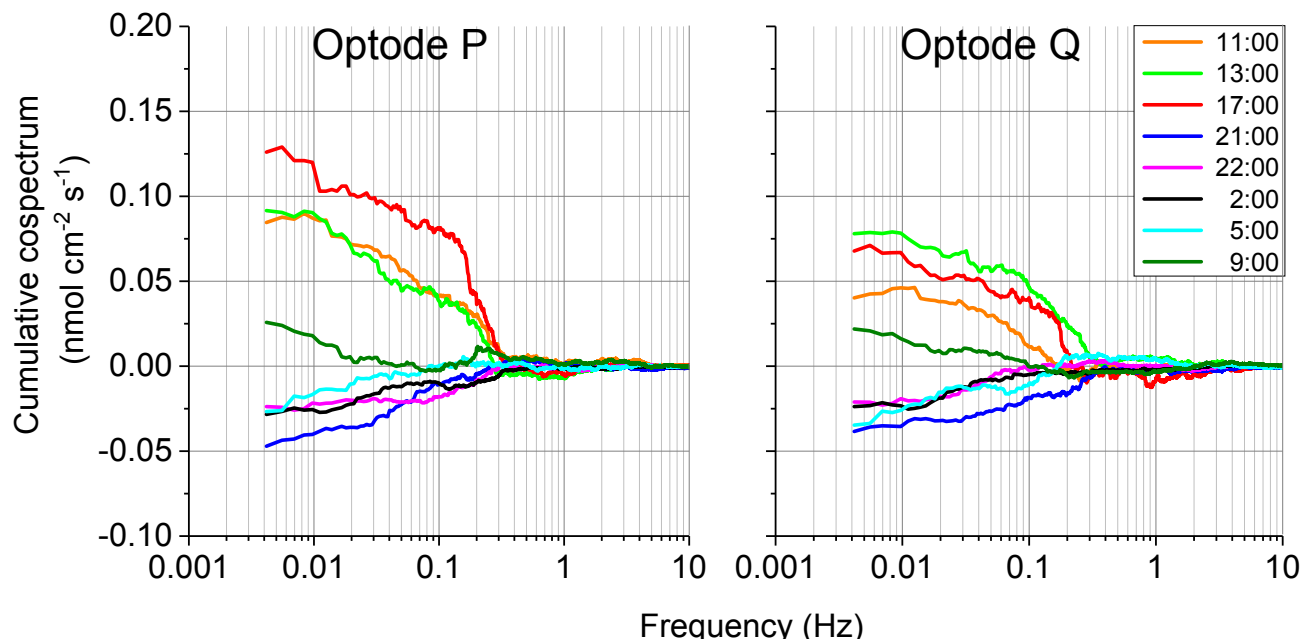


**Figure 3: (A) Comparison between the 15 minute fluxes based on optode P and Q signals for the 16-17 August 2013 deployment. Grey shading depicts the envelope of the measured fluxes except the extreme value at -11, -11 mmol m<sup>-2</sup> h<sup>-1</sup>. B-F: Effects of the corrections applied to the flux calculations on cumulative flux. B: cumulative fluxes calculated from the two optode signals without any correction (raw data). C: Correction for temporal changes in the average water oxygen concentration. D: Time lag correction, E: Correction for wave rotation. F: All corrections used in C, D and E applied and the change in PAR light over time.**



545 **Figure 4: 2OEC deployment of 10-11 April 2014.** Between 15:00 and 18:00, optode P was compromised (likely by marine snow attachment) and this phase was excluded from the calculations for average day and nighttime fluxes. P cumulative flux at 18:00 was intentionally reduced by 5  $\text{mmol m}^{-2}$  to allow comparison of the two cumulative fluxes based on P and Q data (Panel E). For further explanations of the panels see Fig. 2.



550 **Figure 5: 10-11 April 2014 2OEC deployment. Comparison of the cospectra for the two optodes P, Q at 17:00 revealed a steeper slope at the wave frequency 0.2-0.3 Hz. Cospectra processed using the SpectraVer1.2 software (P. Berg).**

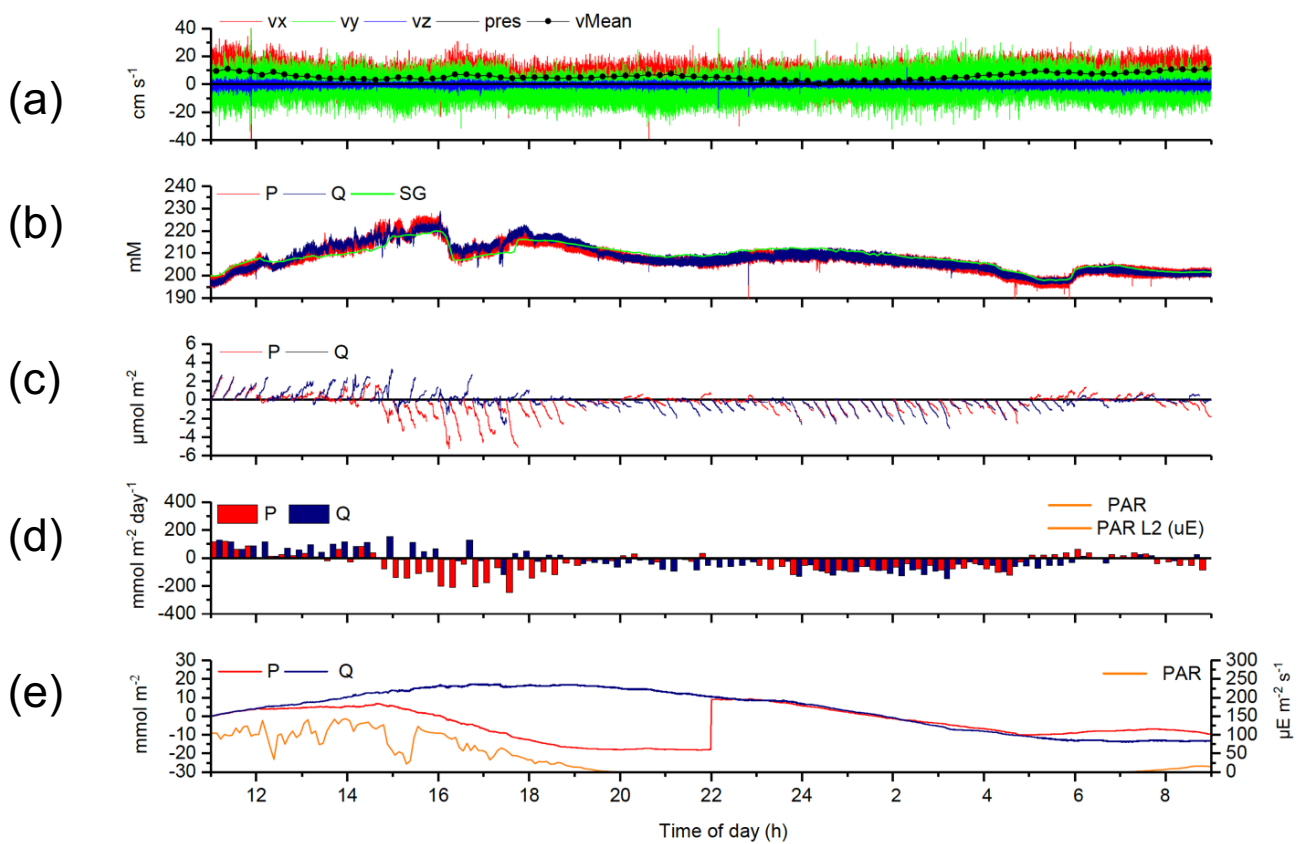
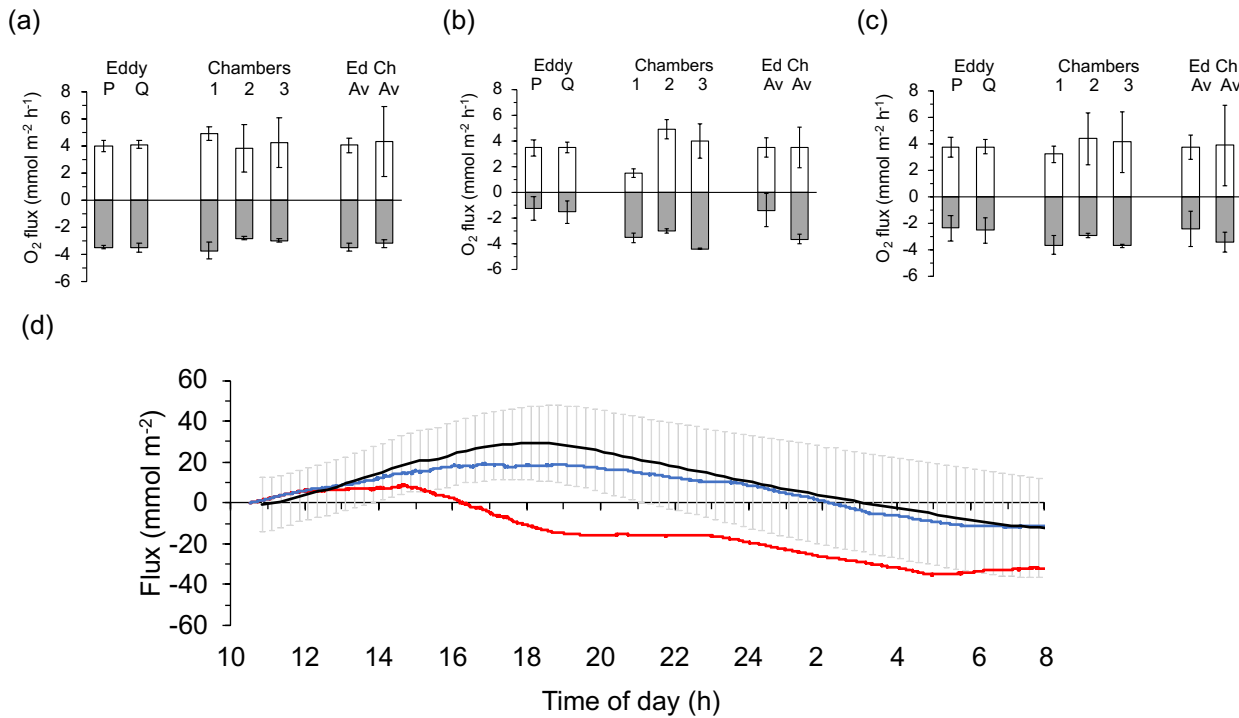


Figure 6: 2OEC deployment of 14-15 August 2013. Between 12:00 and 22:00, optode P was compromised (likely by particle attachment) and again between 5:00 and 9:00 (loss of calibration). These phases were excluded from the calculations for average day and nighttime fluxes. P cumulative flux at 22:00 was intentionally increased by 27 mmol m<sup>-2</sup> to allow comparison of the two cumulative fluxes based on P and Q data (Panel E). For explanations of the panels see Fig. 2.

555

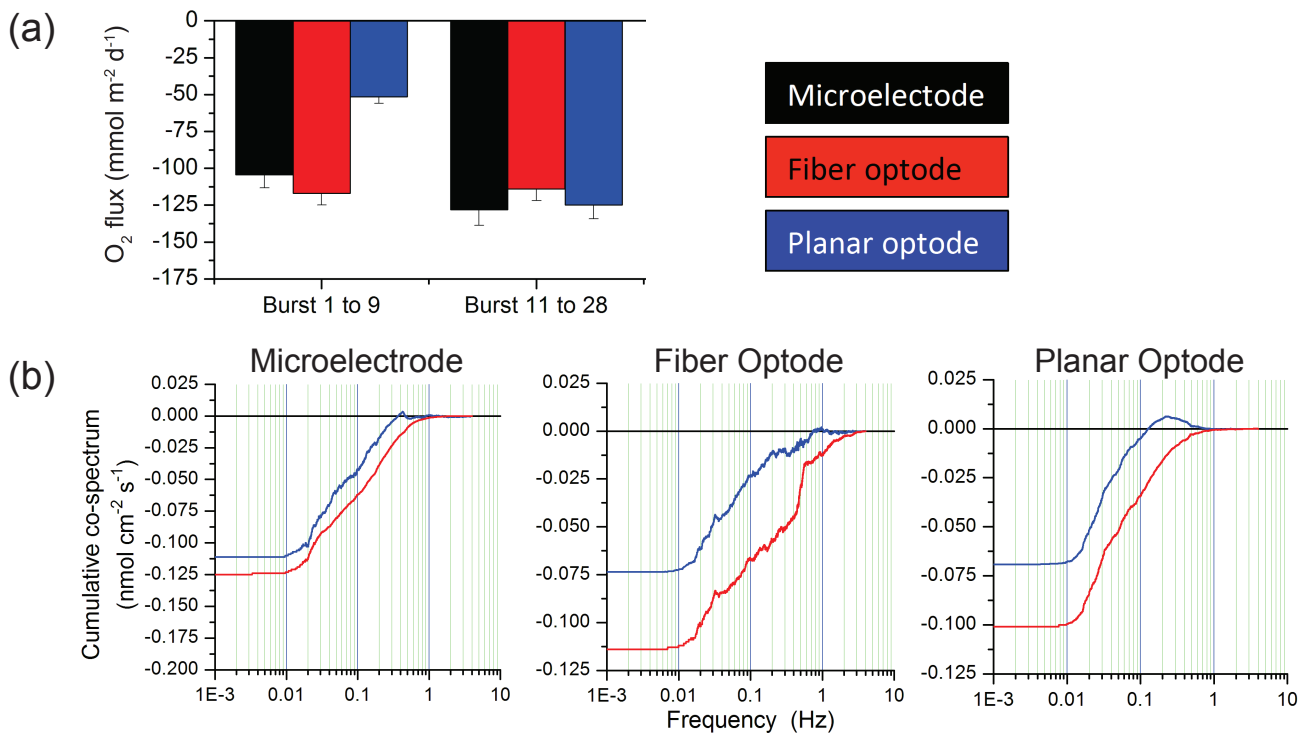
560



565 **Figure 7: Comparison of the day and nighttime fluxes recorded with the eddy covariance instrument and the benthic advection chambers. A: 14-15 August deployments. B: 16-17 August deployments. C: Averages of the two August deployments. Light columns present daytime fluxes, dark columns nighttime fluxes. Error bars depict standard deviation including error propagation. D: Comparison of cumulative flux measured with the chambers (black line) and the 2OEC (red line: optode P, blue line: optode Q) during the 14-15 August deployments. The chamber fluxes confirmed that optode P was temporarily compromised during this deployment. Error bars depict standard deviation.**



570



575 **Figure 8: Comparison of flux estimates generated by eddy covariance instruments equipped with either a Unisense microelectrode, a Pyroscience fiber optode or a Rinko planar optode. A: comparison of time lag corrected fluxes for two burst intervals, each burst 15 minutes long, B: cumulative co-spectra of  $\text{O}_2$  flux vs. frequency for the three sensors. Blue lines represent the uncorrected data, red lines data after time lag correction.**